IEEE Access
Multidisciplinary | Rapid Review | Open Access Journal

Received July 16, 2019, accepted July 21, 2019, date of publication July 30, 2019, date of current version August 14, 2019.

Digital Object Identifier 10.1109/ACCESS.2019.2931933

Investigation of Novel Doubly Salient PM Variable Reluctance Resolvers

QIANG LI, (Member, IEEE), WEI SUN, (Student Member, IEEE), LE SUN, (Member, IEEE), JIAN YU, (Student Member, IEEE), DA XU, (Member, IEEE), XUEFENG JIANG, (Member, IEEE), AND WEIWEI GENG, (Member, IEEE)
School of Automation, Nanjing University of Science and Technology, Nanjing 210094, China
Corresponding author: Wei Sun (sunwei_njust@foxmail.com)

ABSTRACT As rotor position sensors, the variable reluctance (VR) resolvers are playing critical roles in the industrial electric machine drivers. The VR resolvers have a simple structure, therefore, they are reliable and durable under rough operation scenarios. However, the dedicated decoding system requires the voltage signal injection with high-frequency (HF), which must be much higher than the machine operation frequency. The HF injection increases the decoding computation and system cost, especially for the high-speed applications. To avoid applying the HF injection, this paper proposes a new category of VR resolvers by adopting the concept of the doubly salient permanent magnet (PM) motor. The doubly salient PM machines have the magnets and windings on the stator side, thus, they can keep simple and reliable rotors as the VR resolvers. A significant benefit is that the stator-PM can produce back-EMF, which provides the rotor position information. By this way, the HF injection-based VR resolver solution is only serving for low-speeds and can be shut down as long as the PM back-EMF can be detected by the analog circuit. Besides, the proposed linear counterpart is also a novel option for the mover position sensor in the high speed and long distance linear drive system. The modeled examples are analyzed by finite-element analysis (FEA).

INDEX TERMS Doubly salient PM motor, linear drive system, rotor position sensors, variable reluctance resolvers.

I. INTRODUCTION

With simple rotor structure, the variable reluctance (VR) resolver is worldwide popular in the high speed electric machine drive systems [1], [2]. The simple structure makes the VR resolver reliable and robust when facing harsh environments. As a typical example, in the hybrid electric vehicle/electric vehicle (HEV/EV) powertrain, the drive motors are usually operating at high-speeds. Besides, the mechanical vibration is unavoidable in the vehicle, and the electromagnetic interfere (EMI) is terrible in the high voltage drive scenario [3], [4]. The VR resolver is almost a perfect solution for the machine rotor position sensoring and thus has been widely employed in the HEV/EV [5]–[7]. Fig. 1concisely shows the measurement principle of the conventional VR resolver. There is an industrial VR resolver, which is simple and compact, consisting of the stator (stator core and concentrated winding) and rotor (only a core). There are three windings in the stator, i.e. excitation (EXC), sinusoidal (SIN) and cosine (COS) windings. The variable reluctance rotor shape can modulate the amplitude of high-frequency (HF) injection, and the SIN/COS windings consequently generate the back-EMFs as the signals in Fig. 1(b). A resolver decoding circuit samples the HF signals and the processor demodulates them to get the envelopes (the red and blue lines), which are two orthogonal waveforms.

Although such measurement is not that straightforward and requiring time-consuming calculation [8], [9], it can satisfy the regular applications, e.g. a 4 pole-pairs electric machine under 20,000rpm. Sometimes, a separate decoding integrated circuit (IC, e.g. AD2S1210) is employed, which makes cost up.

In recent years, many papers investigated and improved the structure and performance of the VR resolvers. Paper [10] investigated the winding arrangement of the VR resolver and proposed the non-overlapping tooth-coil windings, which can separate the coils and simplify the manufacturing. Paper [11] proposed a novel design of the VR resolver rotor contour, significantly improving the back-EMF waveform shape and the measurement accuracy. Paper [12], [13] extended the

The associate editor coordinating the review of this manuscript and approving it for publication was Xiaodong Sun.

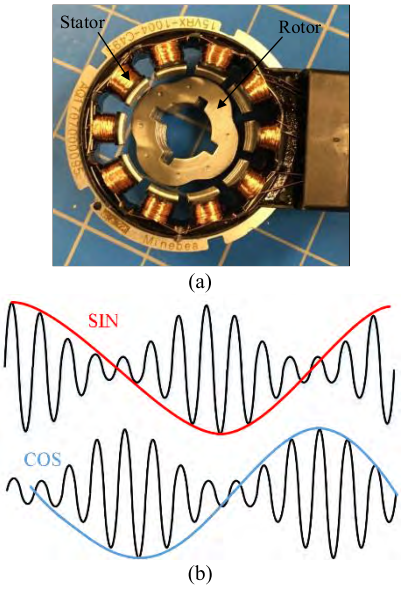

FIGURE 1. The conventional VR resolver for automotive industry. (a) A typical vehicular resolver. (b) The SIN/COS signals.

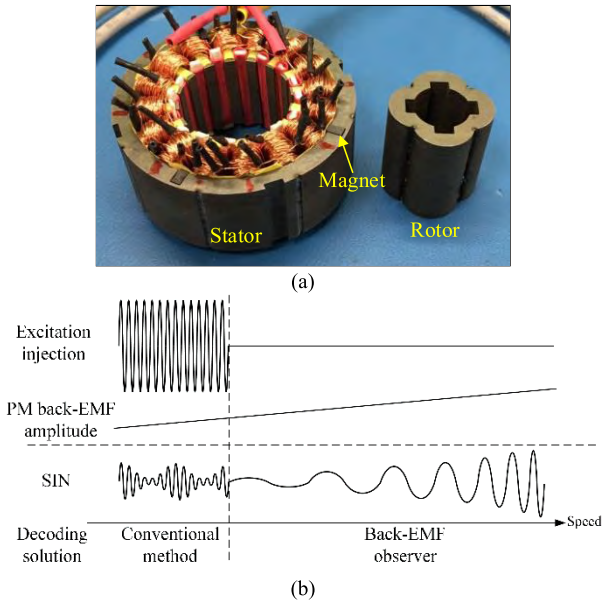

FIGURE 2. The proposed novel doubly salient PM VR resolvers. (a) A prototype. (b) Decoding scheme.

VR resolver to the axial-flux type, and made deep discussion on the winding and slot-poles configurations. Paper [14] discussed the design model of the axial-flux VR resolvers as a general design guidance. Paper [15] analyzed the effect of the parameters on the resolver measurement accuracy.

In the above Fig. 1(b), the frequency must be much higher than the machine operation frequency, i.e. the envelope frequency, otherwise the tracking would be poor. Therefore, with respect to a designated HF frequency, e.g. 10 kHz, there is a speed limit for the operation frequency. For example, in the AD2S1210 solution, the operation frequency cannot be higher than 1kHz (15,000 rpm for a 4 pole-pairs motor) with 12-bit resolution. It is referred to as a frequency-limitation in this paper. To break the frequency-limitation, a possible way is to improve the HF frequency. For example, in [16] and [17], the MHz HF is applied, and even the lamination core can be omitted. But that high HF signals require delicate sample circuits and expensive processors, which cause higher cost, thus unacceptable for the automotive industry.

In the PM motor sensorless control field, the back-EMF observer is a common solution for the rotor position estimation [18]–[20], which provides accurate rotor position especially for high-speed condition, in which the PM back-EMF is significant. However, the regular PM electric machine structure cannot be applied to the VR resolver, because the magnets on the rotor are not able to endure the centrifugal force at super high-speeds. Fortunately, the stator-PM motors come out to be a perfect solution [21], [22]. The stator-PM motor has the magnets on the stator, the magnets thus don't need to suffer any centrifugal force. As a typical stator-PM motor, the doubly salient PM motor has a relatively simple structure [23], in which the rotor structure is exactly the same to that of the regular VR resolver. On basis of this concept, this paper proposes a novel doubly salient PM VR resolver.

Fig. 2(a) shows a prototype of the proposed resolver, consisting of the stator (steel lamination core, winding and magnets) and rotor (only steel lamination core). There is a small amount of ferrite magnet pressed/embedded in the stator core.

Although the PMs are staying in the stator, they can induce PM back-EMFs in the stator windings with the airgap reluctance changing with the rotor rotating. Because the magnet amount is very small, the PM back-EMF is weak at low-speeds. Hence, the HF voltage injection-based position measurement is still required, but only for low-speeds. When the speed is going up, significant back-EMF can be established and used to measure the rotor position. Fig. 2(b) describes this measurement scheme, in which the HF voltage injection stops when the PM back-EMF amplitude is high enough, and this switching point depends on the design of the decoding system. The decoding algorithm also depends on the back-EMF mode. Below the switching point, low-speed mode, the decoding system extracts the envelope of the SIN/COS back-EMFs, and calculates the position with these signals. Above the point, high-speed mode, the decoding system directly calculates the position with the SIN/COS signals. Theoretically, as long as the PM back-EMF can be detected by the analog circuit, even the rotor speed is 1 rpm, the HF injection can be shut off, and switch to the PM back-EMF observer. However, in the real systems, the analog circuit cannot detect the PM back-EMF well if the back-EMF is too weak and noisy. In the system design, the switching point depends on the analog sampling circuit performance. For example, if the analog circuit can only detect stably when the signal amplitude is higher than 0.3V, then the switching point should be determined at a speed point, on which the

PM back-EMF amplitude is 0.3V. By FEA, for the proposed 16/4 resolver, the PM back-EMF amplitude can be around 0.3V at 4500 rpm, thus the speed 4500 rpm is selected as the switching point.

As long as the decoding scheme switches to the high-speed mode, the computational amount becomes small and the HF voltage injection is not required anymore.

On the other hand, this concept can be extended to the linear electric machine drive system as well. The linear position measurement is critical for the linear electric machine drive system, especially in the high-speed railway transportation, where the maglev train is an ideal solution. It is unimaginable to install the conventional linear position sensor on the infinitely long railway [24], [25]. This paper proposes a novel linear variable reluctance (LVR) resolver by using the concept of the doubly salient PM linear motor, in which the magnets and windings are both on the mover and the rail (long stator) structure is simple and low-cost. This novel LVR resolver is actually a two-phase doubly salient PM linear motor, providing two-phase orthogonal back-EMF. By decoding the back-EMF, the mover position can be measured with high accuracy. Comparing with the regular LVR resolver, the decoding computation is much smaller. This feature is particularly suitable for extremely high-speed long-distance railway applications, because the PM back-EMF increases with the moving speed.

Section II proposes the basic structure and principle of the novel VR resolver. An issue of this novel resolver is discussed in Section III. The LVR with the concept of doubly salient PM is introduced in Section IV. Finally, all the analysis in the above sections are validated in Section V by finite-element analysis (FEA).

II. NOVEL VR RESOLVER WITH STATOR-PM STRUCTURE

From the perspective of the PM motor, the proposed VR resolver is essentially a two-phase doubly salient PM motor, producing the two-phase orthogonal back-EMFs.

Fig. 3 illustrates a typical configuration of the proposed VR resolver with 16-slot/4-pole. There are four ferrite magnets mounted on the stator side, constructing four PM poles. One rotor salient pole corresponds to one magnetic pole and spans four stator teeth, which cover a whole electrical period of 360 degree. To make the two-phase orthogonal back-EMFs, the SIN/COS coils are located with a 90 degree phase shift, i.e. the adjacent two stator teeth.

The coil turn numbers of SIN and COS windings are the same. The EXC winding has much less turns, so the EXC winding has less self-inductance. This is because the HF injection in EXC will be turned off at high-speeds, therefore the more slot space should be for the SIN/COS coils, generating orthogonal signals for the whole speed range.

As is shown in Fig. 3, the magnetic circuit is through the stator yoke, teeth, air gap, and the rotor core. The magnetic flux (the dashed curves) is excited by the PMs at high-speeds. However, at low-speeds, or when the PM back-EMF is not significant, the HF voltage injection is required as well.

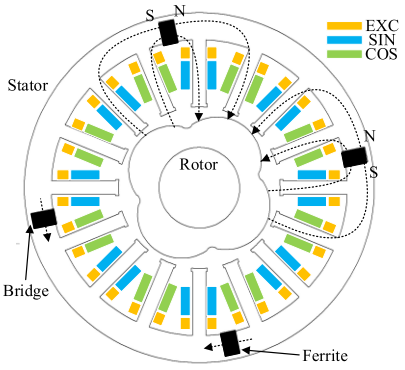

FIGURE 3. A typical configuration of the proposed resolver (16-slot/4-pole).

To simplify the analysis at low-speeds, the PM flux linkage is ignored. In most industrial applications, the excitation is a 10 kHz sinusoidal voltage signal, inducing 10 kHz flux linkage, expressed as:

$$\varphi_{\sin L}(\theta_r, t) = \left[\frac{\lambda_{\max} - \lambda_{\min}}{2}\cos(p_r\theta_r) + \frac{\lambda_{\max} + \lambda_{\min}}{2}\right] F_{EXC}\sin(\omega_{EXC}t) \tag{1}$$

where λ_{max} and λ_{min} are the maximum and minimum airgap permeance, θ_r is rotor position, F_{EXC} is the maximum amplitude of the magneto-motive force (MMF) induced by excitation, p_r is rotor pole number, and ω_{EXC} is the injection angular frequency. The derivation is the same as the COS winding. This flux-linkage is the base for the following derivations, and the item $\cos(p_r\theta_r)$ is critical for the final back-EMF E_{sinL} and E_{sinH}, providing the desired SIN/COS back-EMF components. The assumption is that the airgap permeance is a pure sinusoidal function, so we don't need to consider the harmonics. This assumption is acceptable only when the rotor arc and contour is well designed. Hence, the rotor contour design is a critical work to guarantee the equation (1). And the design procedure is quite similar to the work in [11]. On the other hand, if the rotor arc or contour is not designed well, harmonics will exist in the PM back-EMF, provoking oscillations in the measured position.

The equation (2) essentially explains that the variable air gap is modulating the MMF. By taking the derivative of the flux linkage with respect to time, the induced voltage signal is obtained as:

$$E_{\sin L}(\theta_r, t) = F_{EXC}\frac{\lambda_{\max} - \lambda_{\min}}{2}\{-p_r\omega_r\sin(p_r\theta_r)\sin(\omega_{EXC}t) + \omega_{EXC}[\cos(p_r\theta_r) + \lambda_a]\cos(\omega_{EXC}t)\} \tag{2}$$

where ω_r is the mechanical rotor angular speed and λ_a is defined as:

$$\lambda_a = \frac{\lambda_{\max} + \lambda_{\min}}{\lambda_{\max} - \lambda_{\min}} \tag{3}$$

Considering ω_{EXC} is much higher than $p_r\omega_r$ at low-speeds (for example, ω_{EXC} is 62831 rad/s for 10 kHz, $p_r\omega_r$ is 52 rad/s

at 500 rpm, or 471 rad/s at 4500 rpm), the $p_r\omega_r$ term does not make sense. Hence, the equation (2) can be simplified as:

$$E_{\sin \mathrm{L}}(\theta_r, t) = E_{EXC}[\cos(p_r\theta_r) + \lambda_a]\cos(\omega_{EXC}t) \quad (4)$$

which is plotted in Fig. 4(a), and the E_{EXC} is defined as:

$$E_{EXC} = \omega_{EXC}F_{EXC}\frac{\lambda_{\max} - \lambda_{\min}}{2} \quad (5)$$

With the increase of the rotor speed, the PM back-EMF is becoming significant. After the speed-switching point, the system switches to the high-speed mode, in which the HF injection signal stops. The airgaps under the teeth are always changing with the rotor rotation. Take a SIN tooth as an example, when the rotor salient pole is close to that tooth, the PM flux linkage in that tooth coil is strong, otherwise it is weak. Such a changing PM flux linkage induces the PM back-EMF, which can be expressed as:

$$E_{\sin \mathrm{H}}(\theta_r, t) = E_m \sin(p_r\theta_r) \quad (6)$$

where E_m is defined as:

$$E_m = p_r\omega_r\varphi_m \quad (7)$$

where φ_m is the PM flux linkage amplitude. Fig. 4(b) plots this high-speed component. The magnitude of E_{sinH} is increasing with rotor speeding up. Although the mode switching point is expected to be significant as early as possible (i.e. the E_{sinH} or φ_m should be high), the E_{sinH} should not be out of the sample scale range of the decoding circuit (for example, 0-3V in a regular DSP circuit). Hence, this φ_m depends on the amount of the ferrite magnet, which is a trade-off in the design.

Although the ferrite magnet should be small to limit the cost, it is expensive to machine a tiny size magnet. Besides, the ferrite is very cheap, around $0.0012USD/g, so the magnet size could be big to make the machining easy. The initial width of the magnet is designed as 2mm, which is a size for easy machining. And the initial length of the magnet is selected as the width of the stator yoke, so there is no bridge at the beginning. Then, these width and length need to be adjusted by iterations in FEA. By adding the width of the bridge to 1.5mm (to have a good strength to assemble the stator), the magnet length reduces, the magnet flux concentrate into the bridge due to the short cut magnetic path. Because a lot of magnet flux is lost as flux leakage, the width of the magnet need to increase to have enough PM back-EMF in the SIN/COS windings. By adjusting in the FEA, the magnet width is increased to 2.4mm, by which the PM back-EMF in the SIN/COS winding could be 0.3 V at 4500 rpm.

Regarding future experiments for the cases in this paper, it is easier to get the same size magnet samples from the market. Hence, the 8-slot/3-pole resolver and linear resolver in the following sections will share the same magnet size.

Although the above discussion analyzes the E_{sinL} and E_{sinH} separately, they exist together when the HF injection is on. The actual back-EMF at low-speeds can be exactly expressed as:

$$\begin{aligned} E_{\sin}(\theta_r, t) &= E_{\sin \mathrm{L}} + E_{\sin \mathrm{H}} \\ &= E_{EXC}[\cos(p_r\theta_r) + \lambda_a]\cos(\omega_{EXC}t) + E_m \sin(p_r\theta_r) \end{aligned} \quad (8)$$

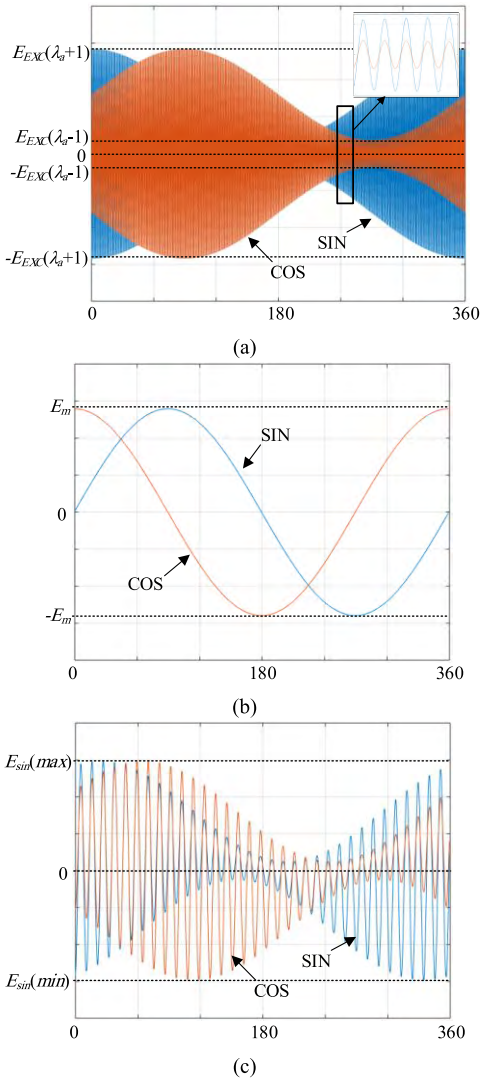

FIGURE 4. Illustration of the operation principle. (a) Plotting E_{sinL} for low-speed mode. (b) Plotting E_{sinH} for high speed mode. (c) Plotting $E_{\sin}$ around the mode switching point.

Fig. 4(c) plots the whole back-EMF E_{sin} around the mode switching point with HF voltage injection. Around this point, no matter the HF voltage injection is on or off, the rotor position can be measured.

There is a practical concern that the PM back-EMF might affect the measurement accuracy at low-speeds. Considering the PM back-EMF item $E_{\sin \mathrm{H}}$ with the demodulation in the

decoding solution, there is:

$$\begin{aligned} &E_{\sin H}(\theta_r, t)\cos(\omega_{EXC}t) \\ &\quad = E_m \sin(p_r\theta_r)\cos(\omega_{EXC}t) \\ &\quad = E_m \sin(p_r\omega_r t)\cos(\omega_{EXC}t) \\ &\quad = \frac{E_m}{2}[\sin((p_r\omega_r + \omega_{EXC})t) + \sin((p_r\omega_r - \omega_{EXC})t)] \end{aligned} \quad (9)$$

There is $p_r\omega_r << \omega_{EXC}$, especially for low-speeds, hence these two above items are both with a high-frequency around ω_{EXC}, which can be removed by a LPF. So the concerned effect is negligible on the low-speed position measurement.

III. NOVEL VR RESOLVER WITH ODD POLES

The proposed doubly salient VR resolver presents a solution for the high-speed position measurement by the PM back-EMF, without requiring any HF injection and demodulation decoding procedures. However, the above structure has a potential issue, which is the PM poles number must be even. This problem is illustrated in this section and the corresponding solution is proposed as well.

A. THE ISSUE OF ODD POLES

As the above proposed VR resolver in Fig. 3, one rotor salient pole is corresponding to one PM pole, spanning over four rotor teeth. By this rule, a 3-pole VR resolver should have the structure as is shown in Fig. 5. The issue comes out that the polarity of the one ferrite magnet cannot be set (the one in the red circle). The root cause is that there is no single-polarity magnet existing in the world.

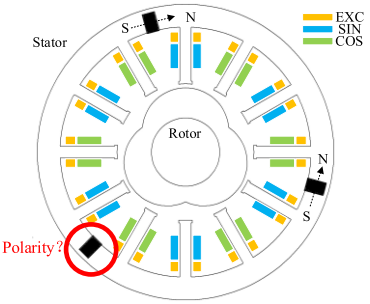

FIGURE 5. The issue the proposed VR resolver when the number of the rotor salient poles is odd (12-slot/3-pole).

Hence, the above proposed doubly salient VR resolver scheme does not provide an entire resolver category. To solve this issue, the magnetic field modulation technology is applied.

B. THE SOLUTION BY FIELD MODULATION TECHNOLOGY

The magnetic field modulation technology can help to combine two magnetic fields with different numbers of poles. The total pole-pair number of the two magnetic fields should equal the number of the modulation blocks. If the salient poles are considered as modulation blocks, this issue can be solved.

Fig. 6 provides a solution for the proposed VR resolver with three salient poles but only one PM pole-pairs

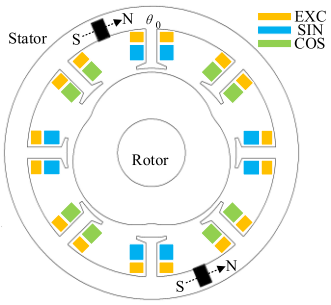

FIGURE 6. The proposed VR resolver with 3 salient poles (8-slot/3-pole).

($p_r = 3$, $p_{\mathrm{PM}} = 1$). With referring to the magnetic flux expression in equation (1), the magnetic field modulation effect is expressed as the product of MMF and permeance, i.e. the flux linkage in the tooth coil at position θ_0.

$$\begin{aligned} \varphi_{\mathrm{PM}}(\theta_0, \theta_r) &= NF_{\mathrm{PM}}(\theta_0)\lambda(\theta_0, \theta_r) \\ &= \frac{\lambda_{\max}-\lambda_{\min}}{2} NF_{\mathrm{PM0}}\cos[p_r(\theta_0-\theta_r)]\sin(p_{\mathrm{PM}}\theta_0) \\ &\quad + \frac{\lambda_{\max}+\lambda_{\min}}{2} NF_{\mathrm{PM0}}\sin(p_{\mathrm{PM}}\theta_0) \end{aligned} \quad (10)$$

The modulated motional back-EMF is the derivative of the flux linkage with respect to time.

$$\begin{aligned} &E_{\mathrm{Mod}}(\theta_0, \theta_r) \\ &\quad = \frac{d\varphi_{\mathrm{PM}}(\theta_0, \theta_r)}{dt} \\ &\quad = NF_{\mathrm{PM0}}\omega_r p_r \frac{\lambda_{\max}-\lambda_{\min}}{2}\sin[p_r(\theta_0-\theta_r)]\sin(p_{\mathrm{PM}}\theta_0) \\ &\quad = E_{\mathrm{PM0}}\cos[(p_r - p_{\mathrm{PM}})(\theta_0 - \frac{p_r\omega_r}{p_r - p_{\mathrm{PM}}}t)] \\ &\qquad - E_{\mathrm{PM0}}\cos[(p_r + p_{\mathrm{PM}})(\theta_0 - \frac{p_r\omega_r}{p_r + p_{\mathrm{PM}}}t)] \end{aligned} \quad (11)$$

As an example case for the odd pole resolver, rotor pole number $p_r = 3$. To use as less PM as possible, only one PM pole pair is adopted, hence $p_{PM} = 1$. Hence, the two terms of equation (11) represent two options of the winding configuration, i. e. $p_r + p_{PM}$ (= 4 pole-pairs), or $p_r - p_{PM}$ (= 2 pole-pairs). However, for a stator with 8 teeth/slots, the option of 4 pole pairs is impossible for a two-phase motor. Therefore, the 2 pole-pair ($p_w = p_r - p_{PM}$) configuration is selected for the SIN/COS windings. By similar derivation as (1) - (8), the expressions of E_{sinL}, E_{sinH}, and E_{sin} can be obtained. Fig. 7 plots these back-EMFs.

Comparing Fig. 4 with Fig. 7, there are two significant differences worthy to be noted. The first is observed in Fig. 4(a) and Fig. 7(a). The envelopes of SIN/COS only stay on one side of the 0-axis in Fig. 4(a). But they can go across the 0-axis in Fig. 7(a). There is a DC-bias magnetization in the four teeth under the same PM pole. In equation (1), the flux linkage has a constant term, i.e. $(\lambda_{max} + \lambda_{min})/2$, which can explain that DC-bias, which is also mentioned in doubly salient motor paper [26]. But this DC-bias does not exist in the 8-slot/3-pole resolver. The second can be

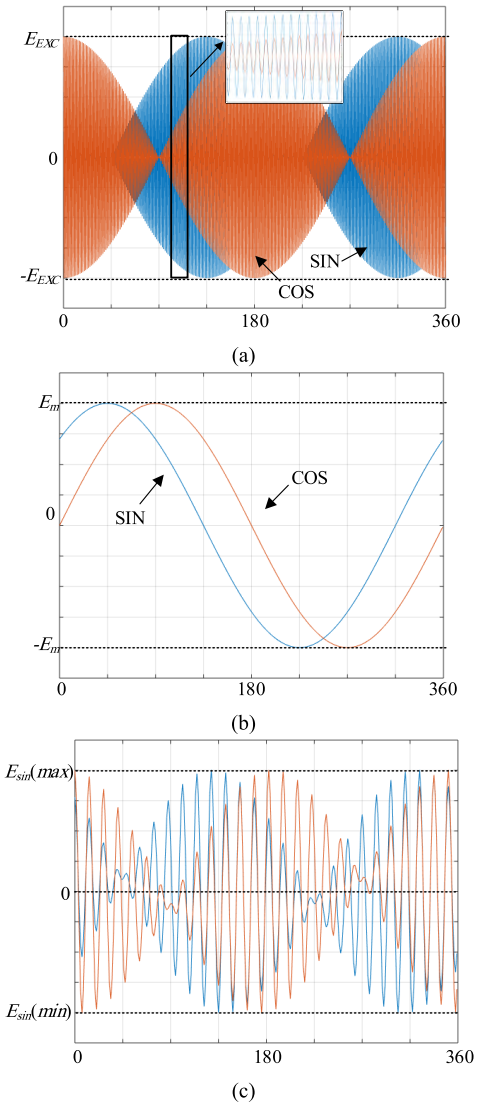

FIGURE 7. Illustration of the proposed VR resolver with 3 rotor poles. (a) Plotting E_{sinL} for low-speed mode. (b) Plotting E_{sinH} for high speed mode. (c) Plotting E_{sin} around the mode switching point.

observed in Fig. 4(b) and Fig. 7(b). The SIN/COS signals are strictly orthogonal in Fig. 4(b), which is perfect for position measurement. However, they are not orthogonal in Fig. 7(b), but with 45° electrical angle shift with respect to each other (named as quasi-orthogonal signals in this paper). To use these two quasi-orthogonal signals to measure rotor position, there must be a pre-transformation. Consider the waveform in Fig. 7(b), in which the $E_{\sin H}$ and $E_{\cos H}$ can be written as:

$$\begin{cases} E_{\sin H}(t) = E_H \sin(3\omega_r t + \dfrac{\pi}{4}) \\ E_{\cos H}(t) = E_H \sin(3\omega_r t) \end{cases} \tag{12}$$

Then, the pre-transformation can make them become two orthogonal signals, i.e.

$$\begin{cases} E'_{\sin H}(t) = E_H \sin(3\omega_r t) \\ E'_{\cos H}(t) = \sqrt{2}E_{\sin H} - E_{\cos H} = E_H \cos(3\omega_r t) \end{cases} \tag{13}$$

IV. NOVEL LINEAR VR RESOLVER

In terms of long distance railway direct drive system, the linear grating encoder and linear variable differential transformer (LVDT) are costly options, the conventional VR resolvers is not well supportive for super-high-speed scenario, e.g. maglev train and hyper-loop bus, in which the extremely HF injection will be required. The proposed novel resolver concept can be implemented on the linear electric machine drive system. The PM back-EMF is inherently suitable for this super-high-speed application. Only a limited amount of ferrite magnet is required on the primary side (mover).

As mentioned above, there are two options for the linear VR resolver structure, i.e. the 16-slot/4-pole and 8-slot/3-pole. From the perspective of the linear resolver, both of them have four teeth under one PM polarity. The difference is the railway pole number under one PM polarity, 1:1 or 1.5:1. This point determines the back-EMFs angle shift between the SIN/COS windings, orthogonal or quasi-orthogonal. Because the orthogonal signals are easier for position measurement, the 1:1 scheme is recommended in this paper, as is shown in Fig. 8.

V. FINITE ELEMENT ANALYSIS AND VALIDATION

The FEA tool is employed to analyze the flux distribution in the resolvers. Table 1 presents the general dimension parameters of the resolvers. The railway of the linear VR resolver is made of regular steel, same to the material of the train railway. Hence, in actual application, the surface of the train railway can be machined to form the VR resolver secondary side, the cost thus will not increase by this way. As is mentioned before, the three resolvers share the same magnet size. Although the linear resolver is straight and the 16/4 resolver is with a circular shape, the mover size of the linear resolver is similar to the stator size of the 16/4 resolver. So the costs of them are also similar. The length and height of the mover are 130mm and 13mm respectively. Actually, the linear resolver is even cheaper, because the rail (secondary side) is made of regular steel, which is the same as the railway material.

TABLE 1. Dimension parameters of the proposed VR resolvers.

Poles number	Even	Odd
Stator slots/rotor poles	16/4	8/3
Stator outer diameters (mm)	52	52
Axial length (mm)	20	20
Air-gap length (mm)	0.7 (min)	0.7 (min)*
Coil size (AWG)	32	32
Ferrite amount (g)	3	1.5

* The mover dimension parameters of the linear VR resolver are similar to that of the 16/4 rotary resolver, but with linear structure.

A. FEA EVALUATION OF THE DOUBLY SALIENT VR RESOLVER

Fig. 9(a) shows the flux distribution in the 16/4 resolver. As the flux distributions in Fig. 9, the feature of the flux path is shown, most of the flux bypass the teeth but go through

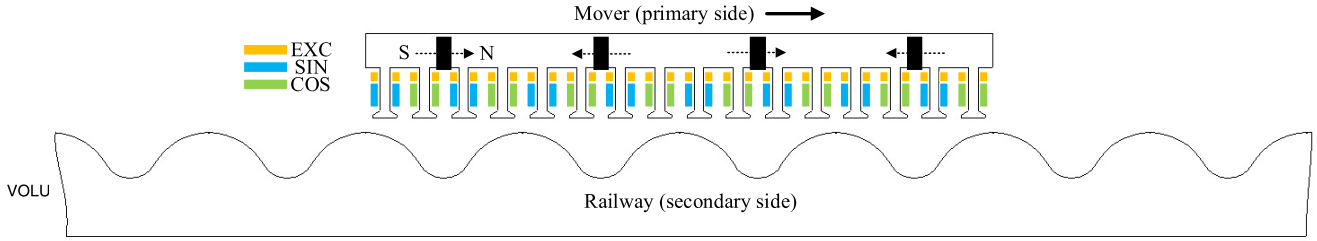

FIGURE 8. The proposed novel linear VR resolver.

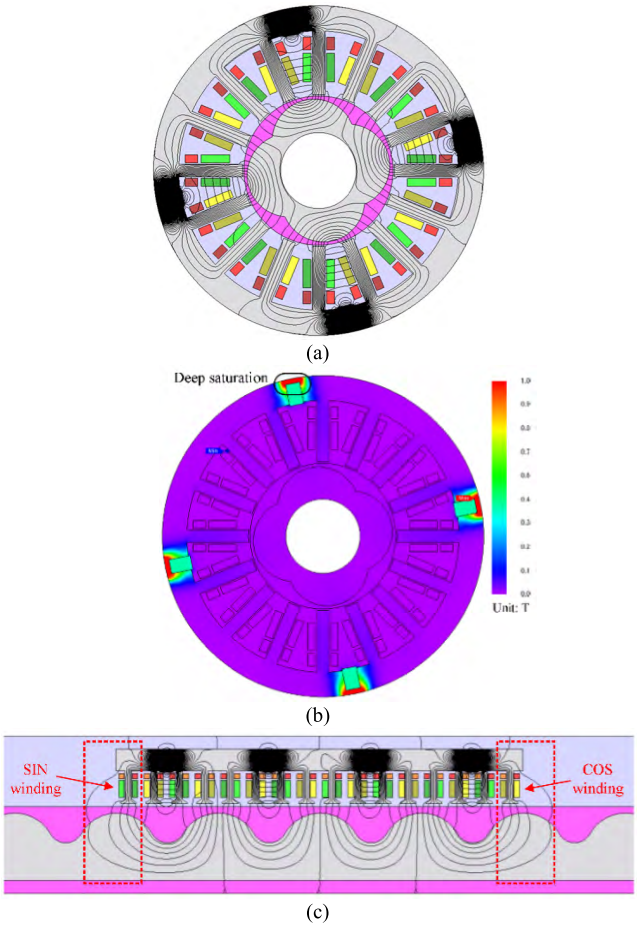

FIGURE 9. FEA results for the flux distribution in the 16/4 VR resolver and linear resolver. (a) Flux distribution in the 16/4 resolver. (b) Flux density distribution in the 16/4 resolver. (c) Flux distribution of the proposed linear resolver.

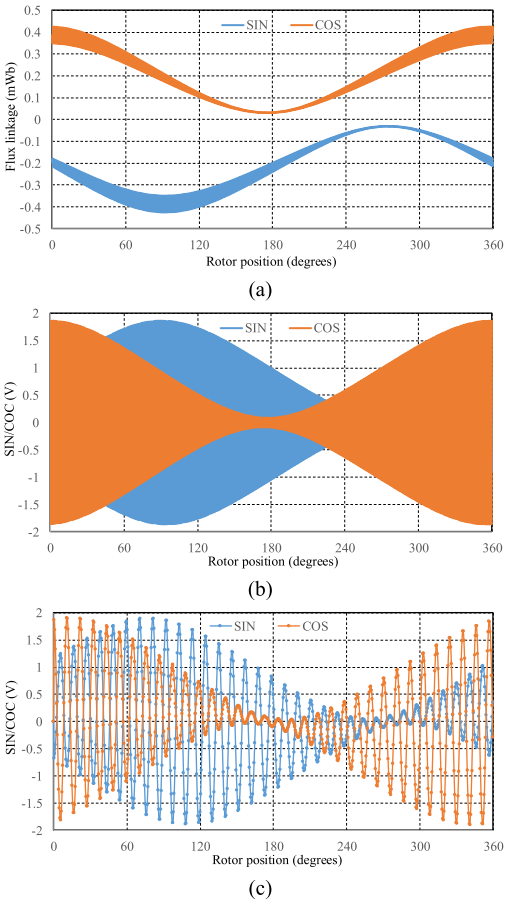

FIGURE 10. FEA results for low-speed conditions (16-slot/4-pole resolver). (a) Flux linkage at 500 rpm. (b) SIN/COS signals for 500 rpm. (c) SIN/COS signals for 4,500 rpm.

the bridge of the stator yoke, only a few goes through the coils on the teeth. In Fig. 9(b), the stator yoke bridge is in deep saturation, but most part of the resolver is staying under unsaturation. The PM amount can be saved by reducing the thickness of the stator yoke bridge or even eliminating it, but it would complicate the manufacturing. So the bridge is only for the convenience of the stator assembling, as long as the mechanical strength is enough, the bridge size is acceptable. The drawback of the bridge is the flux leakage caused by the flux short cut, so more ferrite will be required to strengthen the PM back-EMF.

Considering the ferrite is cheap, the bridge is retained. Because the teeth and rotor always stay in unsaturation, the waveform shapes of SIN/COS signals won't deform in all conditions. This phenomenon exits in the linear resolver as well, as is shown in Fig. 9(c). The end-effect, which means the flux leakage on the two ends of the linear machine is distinct to the central part (as is shown in the red dished frame in Fig. 9c), is a unique feature in the linear machines. This effect might provoke torque ripple in the regular three-

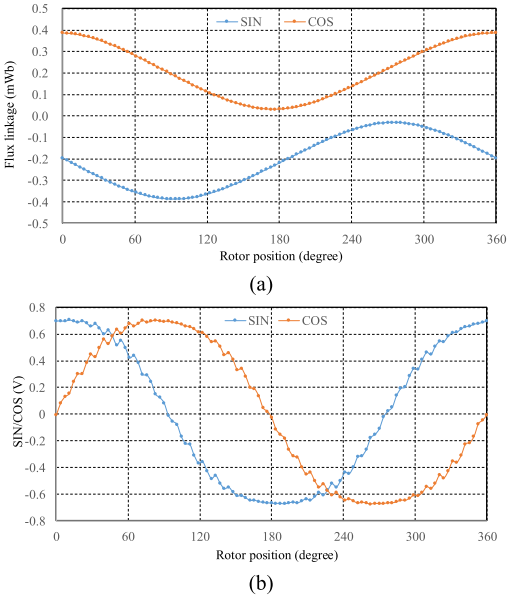

FIGURE 11. FEA results for a high-speed condition (16-slot/4-pole resolver). (a) Flux linkage at 10,000 rpm. (b) SIN/COS signals for 10,000 rpm.

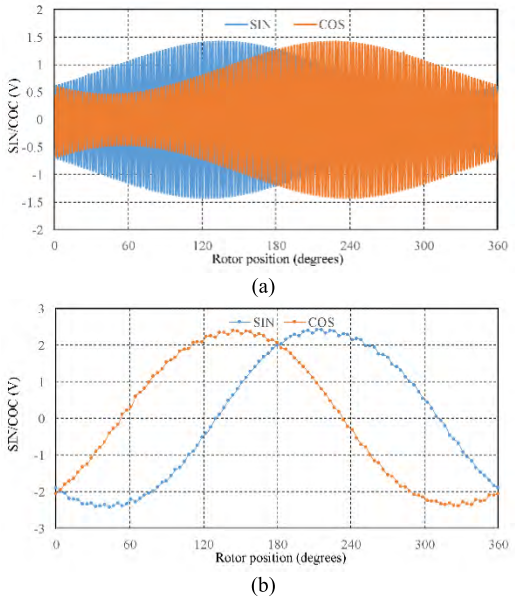

FIGURE 12. FEA results for the proposed linear resolver back-EMFs (one rail poles is corresponding 360 elec. deg.). (a) Signals (HF back-EMFs) at 2.16 m/s. (b) PM back-EMFs at 108 m/s.

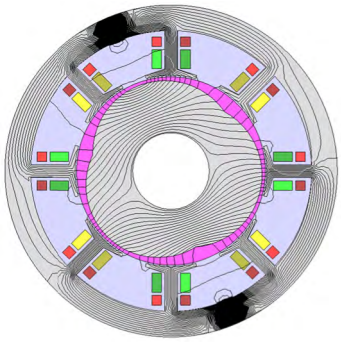

FIGURE 13. FEA results for the flux distribution in the 8/3 VR resolver.

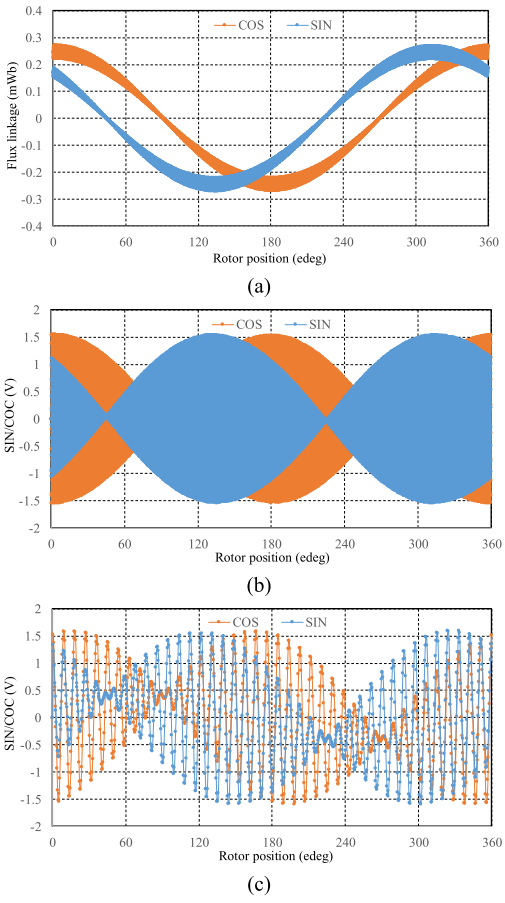

FIGURE 14. FEA results for low-speed conditions (8-slot/3-pole resolver). (a) Flux linkage at 500 rpm. (b) SIN/COS signals for 500 rpm. (c) SIN/COS signals for 5,000 rpm.

phase machines, for the sake that only two of the three phases have this special flux leakage, so the asymmetry exists in the windings. But this problem does not occur in the linear resolver, which has only two phase windings, i.e. the SIN/COS windings.

Although part of the core is suffering severe saturation and flux leakage, these conditions are consistent along the whole speed range. Hence, theoretically, as long as the proposed resolver is calibrated well at some single speed point, the resolver can keep a good accuracy in the whole speed range.

Fig. 10 shows the flux linkages and back-EMFs in the SIN/COS windings at low-speed mode, with which the 10 kHz HF voltage injection is imposed in the EXC winding. Fig. 10(a) shows the flux linkages, which are staying on the two separate sides of the 0-axis. This is because the PM locks the magnetization direction in the teeth. It is also the DC-bias mentioned above. Fig. 10(b) and (c) show the

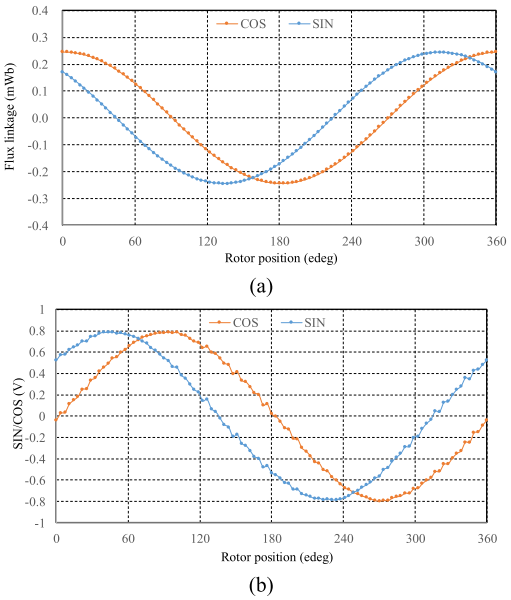

FIGURE 15. FEA results for a high-speed condition (8-slot/3-pole resolver). (a) Flux linkage at 10,000 rpm. (b) SIN/COS signals for 10,000 rpm.

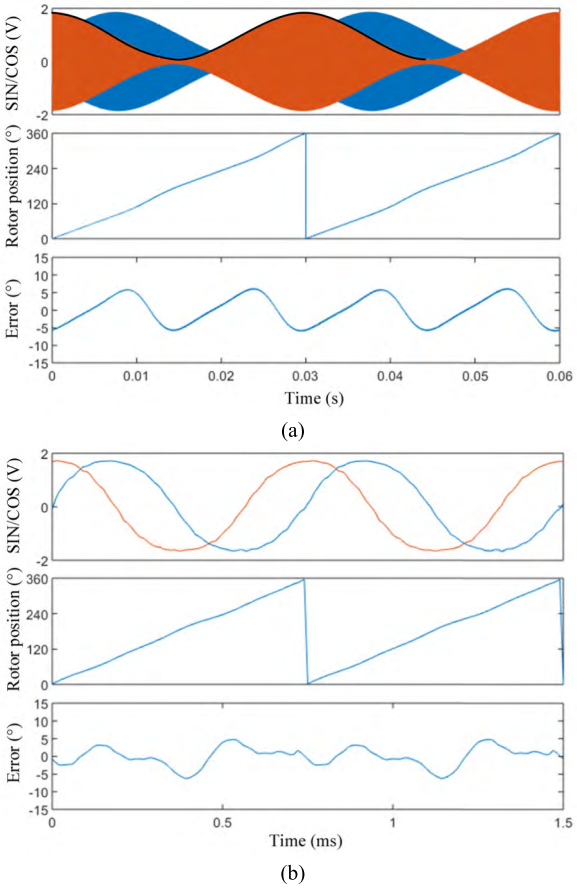

FIGURE 16. Position measurement evaluation for the 16-slot/4-pole resolver. (a) Evaluation at 500 rpm. (b) Evaluation at 20,000 rpm.

back-EMFs at 500 rpm and 4,500 rpm, corresponding to the Fig. 4(a) and (c). The FEA results agree well with the analysis results.

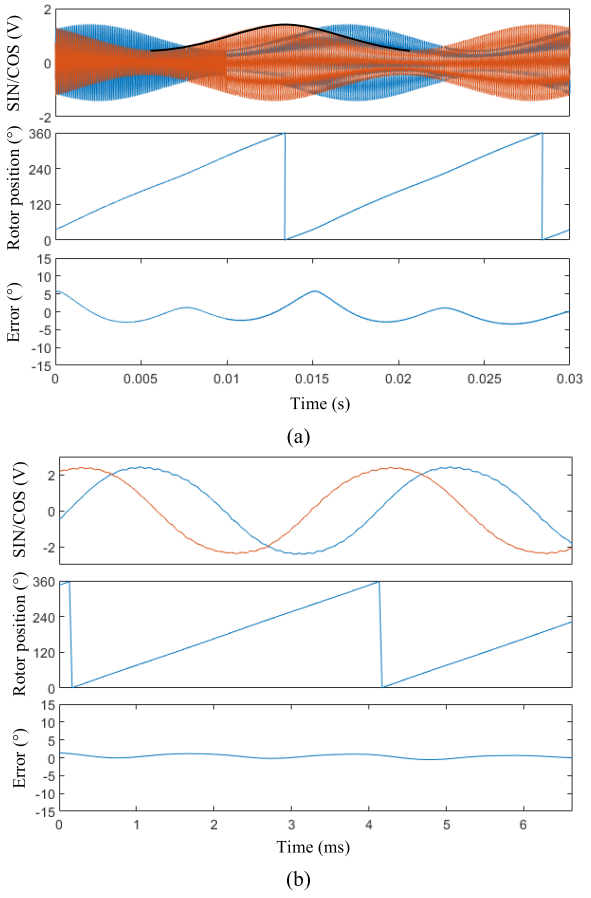

FIGURE 17. Position measurement evaluation for the linear resolver. (a) Evaluation at 2.16 m/s. (b) Evaluation a 108 m/s.

In terms of the high-speed mode, Fig. 11 plots the flux linkages and back-EMFs in the SIN/COS windings at 10,000 rpm, when the HF injection is off. Comparing with Fig. 10(a), the flux linkage in Fig. 11(a) has only the low-frequency component (667 Hz), separated into the two sides of 0-axis.

In Fig. 11(b), the two-phase SIN/COS back-EMFs are strictly orthogonal, which can be directly applied to calculate the rotor position. The analysis in Fig. 4(b) is verified in this Fig. 11(b).

By the FEA model in Fig. 9(c), the back-EMFs in the linear resolver are calculated at 2.16m/s (7.8 km/h) and 108 m/s (389 km/h) respectively. Fig. 12 shows the back-EMFs. The waveforms are similar to those in Fig. 10(b) and Fig. 11(b).

B. EFFECT OF THE FIELD MODULATION

Fig. 13 shows the flux distribution in the 8/3 doubly salient VR resolver. The deep saturation occurs again around the magnets slots, i.e. the bridge area. Unlike the 16/4 resolver, the flux distribution in this 3-pole rotor is asymmetrical. But the flux linkages in the SIN/COS windings are symmetrical, as is shown in Fig. 14 (a). Fig. 14(b) and (c) show the back-EMFs at 500 rpm and 5,000 rpm respectively.

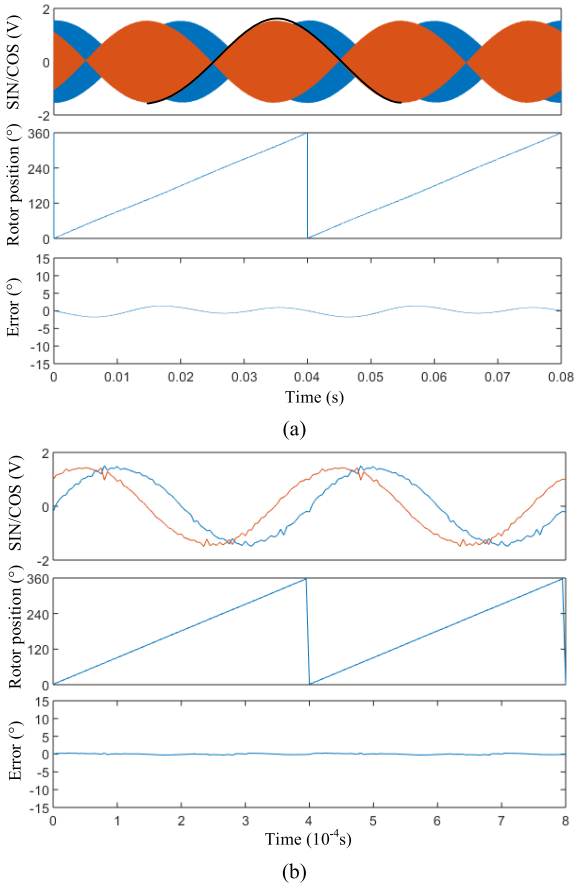

FIGURE 18. Position measurement evaluation for the 8-slot/3-pole resolver. (a) Evaluation at 500 rpm. (b) Evaluation for 25,000 rpm.

By 10 kHz HF injection, the SIN/COS back-EMFs are with 45° angle shift with respect to each other, verifying the analysis in Fig. 7.

With turning off the HF injection, Fig. 15 shows the PM flux linkages and PM back-EMFs in the windings at 10,000 rpm, when the back-EMF amplitude has been significant enough to be detected. All the FEA results agree well with the formula derivation before. The next step is to use them to calculate the rotor position.

C. POSITION MEASUREMENT EVALUATION

In the real system, the processor samples the back-EMFs as position signals, and calculates the rotor position on basis of the information included in those signals.

In this paper, this process can be simulated in Matlab/Simulink. The FEA results of the back-EMFs are imported to Matlab, where the decoding logic calculates the rotor position. First is the 16/4 doubly salient PM VR resolver, in Fig. 16(a), the HF back-EMFs are demodulated to work out the signal envelopes, which are two-phase orthogonal waveforms. Because the envelopes are staying in one side of the 0-axis, a subtraction has to be applied to move them to the center of the Y-axis. Below the HF signals, the rotor position and measurement errors are evaluated.

For high-speeds, the calculation is easier, as importing the high-speed PM back-EMFs from FEA, the high-speed rotor position can be directly calculated in Fig. 16(b), and the error is evaluated below.

Because the configuration of the linear resolver is the same as the 16/3 resolver, the back-EMFs and measurement performances are similar as well, as is shown in Fig. 17. The measurement presents similar features as those of the 16/4 resolver.

Fig. 18(a) and (b) show the position measurement for the 8/3 VR resolver, including the low-speed mode and the high-speed mode.

With respect to the 8/3 VR resolver, the processing is similar to that of the 16/4 resolver, the HF back-EMFs are demodulated at low-speeds as well. But the signal envelopes are separated into the two sides of the 0-axis, so the signal subtraction is not needed.

In low-speed mode, the 16/4 resolver error is around 5°, but the 8/3 resolver error is less than 2°. In high-speed mode, the 8/3 resolver error comes to be even smaller, around 0.5°. The 16/4 resolver apparently has more error than that of the 8/3 resolver. This is because the 16/4 resolver flux linkage has DC-bias in the, as is shown in Fig. 10(a) and Fig. 11(a), which makes the expected sinusoidal waveform deformed.

The FEA and simulation evaluation has illustrated that, compared with the proposed 16/4 resolver, the proposed 8/3 VR resolver with filed modulation technology can present better position measurement, but using less magnets.

VI. CONCLUSION

This paper proposes a novel category of the VR resolvers, combining the doubly salient PM motor concept and the conventional VR resolvers. The main contribution of this concept is that the PM back-EMF can be applied to solve the rotor position measurement for high-speed motor control while inheriting the simple and firm rotor structure from the conventional VR resolver, the conventional and complicated HF injection-based decoding solution is only required at the low speeds though.

The issue of the odd poles number is noted, illustrated and solved by the field modulation principle. A complete series of the proposed doubly salient PM VR resolvers, including the rotary and linear resolvers with different slot-pole configurations, are presented and discussed.

The FEA is applied to analyze the resolvers, verifying the principle analysis. The FEA results are imported to the Matlab/Simulink, where the position measurement and errors are evaluated. The prototypes of the proposed resolvers are under manufacturing, and related experimental work will be reported in future.

REFERENCES

[1] L. Sun, "Analysis and improvement on the structure of variable reluctance resolvers," *IEEE Trans. Magn.*, vol. 44, no. 8, pp. 2002–2008, Aug. 2008.
[2] L. Ben-Brahim, M. Benammar, and M. A. Alhamadi, "A resolver angle estimator based on its excitation signal," *IEEE Trans. Ind. Electron.*, vol. 56, no. 2, pp. 574–580, Feb. 2009.

[3] F. L. Mapelli, D. Tarsitano, and M. Mauri, "Plug-in hybrid electric vehicle: Modeling, prototype realization, and inverter losses reduction analysis," *IEEE Trans. Ind. Electron.*, vol. 57, no. 2, pp. 598–607, Feb. 2010.

[4] X. Ge, Z. Q. Zhu, R. Ren, and J. T. Chen, "A novel variable reluctance resolver for HEV/EV applications," *IEEE Trans. Ind. Appl.*, vol. 52, no. 4, pp. 2872–2880, Jul./Aug. 2016.

[5] X. Sun, C. Hu, G. Lei, Y. Guo, and J. Zhu, "State feedback control for a PM hub motor based on grey wolf optimization algorithm," *IEEE Trans. Power Electron.*, to be published. doi: 10.1109/TPEL.2019.2923726.

[6] X. Sun, K. Diao, G. Lei, Y. Guo, and J. Zhu, "Study on segmented-rotor switched reluctance motors with different rotor pole numbers for BSG system of hybrid electric vehicles," *IEEE Trans. Veh. Technol.*, vol. 68, no. 6, pp. 5537–5547, Jun. 2019.

[7] Z. Shi, X. Sun, Y. Cai, Z. Yang, G. Lei, Y. Guo, and J. Zhu, "Torque analysis and dynamic performance improvement of a PMSM for EVs by skew angle optimization," *IEEE Trans. Appl. Supercond.*, vol. 29, no. 2, pp. 1–5, Mar. 2019.

[8] M. Benammar, L. Ben-Brahim, and M. A. Alhamadi, "A high precision resolver-to-DC converter," *IEEE Trans. Instrum. Meas.*, vol. 54, no. 6, pp. 2289–2296, Dec. 2005.

[9] S. Sarma, V. K. Agrawal, and S. Udupa, "Software-based resolver-to-digital conversion using a DSP," *IEEE Trans. Ind. Electron.*, vol. 55, no. 1, pp. 371–379, Jan. 2008.

[10] X. Ge, Z. Q. Zhu, R. Ren, and J. T. Chen, "A novel variable reluctance resolver with nonoverlapping tooth–coil windings," *IEEE Trans. Energy Convers.*, vol. 30, no. 2, pp. 784–794, Jun. 2015.

[11] X. Ge and Z. Q. Zhu, "A novel design of rotor contour for variable reluctance resolver by injecting auxiliary air-gap permeance harmonics," *IEEE Trans. Energy Convers.*, vol. 31, no. 1, pp. 345–353, Mar. 2016.

[12] R. Alipour-Sarabi, Z. Nasiri-Gheidari, F. Tootoonchian, and H. Oraee, "Analysis of winding configurations and slot-pole combinations in fractional-slots resolvers," *IEEE Sensors J.*, vol. 17, no. 14, pp. 4420–4428, Jul. 2017.

[13] R. Alipour-Sarabi, Z. Nasiri-Gheidari, F. Tootoonchian, and H. Oraee, "Improved winding proposal for wound rotor resolver using genetic algorithm and winding function approach," *IEEE Trans. Ind. Electron.*, vol. 66, no. 2, pp. 1325–1334, Feb. 2019.

[14] H. Saneie, Z. Nasiri-Gheidari, and F. Tootoonchian, "Design-oriented modelling of axial-flux variable-reluctance resolver based on magnetic equivalent circuits and Schwarz–Christoffel mapping," *IEEE Trans. Ind. Electron.*, vol. 65, no. 5, pp. 4322–4330, May 2018.

[15] R. Alipour-Sarabi, Z. Nasiri-Gheidari, F. Tootoonchian, and H. Oraee, "Effects of physical parameters on the accuracy of axial flux resolvers," *IEEE Trans. Magn.*, vol. 53, no. 4, Apr. 2017, Art. no. 8101211.

[16] Z. Zhang, F. Ni, Y. Dong, C. Guo, M. Jin, and H. Liu, "A novel absolute magnetic rotary sensor," *IEEE Trans. Ind. Electron.*, vol. 62, no. 7, pp. 4408–4419, Jul. 2015.

[17] B. Aschenbrenner and B. G. Zagar, "Analysis and validation of a planar high-frequency contactless absolute inductive position sensor," *IEEE Trans. Instrum. Meas.*, vol. 64, no. 3, pp. 768–775, Mar. 2015.

[18] Z. Chen, M. Tomita, S. Doki, and S. Okuma, "An extended electromotive force model for sensorless control of interior permanent-magnet synchronous motors," *IEEE Trans. Ind. Electron.*, vol. 50, no. 2, pp. 288–295, Apr. 2003.

[19] S. Nalakath, Y. Sun, M. Preindl, and A. Emadi, "Optimization-based position sensorless finite control set model predictive control for IPMSMs," *IEEE Trans. Power Electron.*, vol. 33, no. 10, pp. 8672–8682, Oct. 2018.

[20] X. Sun, L. Chen, Z. Yang, and H. Zhu, "Speed-sensorless vector control of a bearingless induction motor with artificial neural network inverse speed observer," *IEEE/ASME Trans. Mechatronics*, vol. 18, no. 4, pp. 1357–1366, Aug. 2013.

[21] W. Hua, M. Cheng, Z. Q. Zhu, and D. Howe, "Analysis and optimization of back EMF waveform of a flux-switching permanent magnet motor," *IEEE Trans. Energy Convers.*, vol. 23, no. 3, pp. 727–733, Sep. 2008.

[22] R. Cao, C. Mi, and M. Cheng, "Quantitative comparison of flux-switching permanent-magnet motors with interior permanent magnet motor for EV, HEV, and PHEV applications," *IEEE Trans. Magn.*, vol. 48, no. 8, pp. 2374–2384, Aug. 2012.

[23] M. Cheng, K. T. Chau, and C. C. Chan, "Static characteristics of a new doubly salient permanent magnet motor," *IEEE Trans. Energy Convers.*, vol. 16, no. 1, pp. 20–25, Mar. 2001.

[24] A. Daniar, Z. Nasiri-Gheidari, and F. Tootoonchian, "Performance analysis of linear variable reluctance resolvers based on an improved winding function approach," *IEEE Trans. Energy Convers.*, vol. 33, no. 3, pp. 1422–1430, Sep. 2018.

[25] Z. Nasiri-Gheidari, "Design, performance analysis, and prototyping of linear resolvers," *IEEE Trans. Energy Convers.*, vol. 32, no. 4, pp. 1376–1385, Dec. 2017.

[26] S. Zhu, M. Cheng, J. Dong, and J. Du, "Core loss analysis and calculation of stator permanent-magnet machine considering DC-biased magnetic induction," *IEEE Trans. Ind. Electron.*, vol. 61, no. 10, pp. 5203–5212, Oct. 2014.

QIANG LI was born in Jiangsu, China, in 1969. He received the B.S. degree from the Harbin Institute of Technology (HIT), Harbin, China, in 1992, and the Ph.D. degree in electrical engineering from Southeast University, Nanjing, China, in 2005.

In 2005, he joined the Department of Electrical Engineering, School of Automation, Nanjing University of Science and Technology (NJUST), where he has been engaged in teaching and research in the field of electrical engineering. His main research interests include electric motor design, motor control, switching mode power supply, and embedded systems.

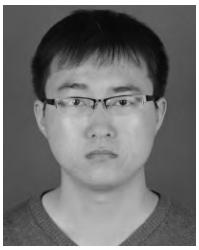

WEI SUN was born in Jiangsu, China, in 1992. He received the B.S. degree in electrical engineering from the Nanjing University of Science and Technology (NJUST), Nanjing, China, in 2014, where he is currently pursuing the Ph.D. degree with the School of Automation.

His main research interest includes electric motor design and control.

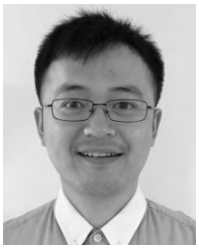

LE SUN (S'15–M'17) received the B.S. and M.S. degrees from the Nanjing University of Aeronautics and Astronautics, Nanjing, China, in 2009 and 2012, respectively, and the Ph.D. degree in electrical engineering from the School of Electrical Engineering, Southeast University, Nanjing, in 2016.

From 2012 to 2013, he was a R&D Engineer with United Automotive Electronic Systems Company, Ltd., Shanghai. From 2016 to 2018, he was with the McMaster Automotive Resource Centre, McMaster University, where he was leading a research team of the motor control technologies. He is currently an Associate Professor with the Department of Electrical Engineering, Nanjing University of Science and Technology (NJUST), Nanjing. His research interest includes analysis, design, and control of permanent-magnet motors and power management techniques for electric vehicle (EV) and hybrid EV applications.

JIAN YU received the B.S. degree from Jianghan University, Wuhan, China, in 2003, and the M.S. degree from East China Jiaotong University, Nanchang, China, in 2007. He is currently pursuing the Ph.D. degree with the Department of Electrical Engineering, Nanjing University of Science and Technology (NJUST), Nanjing, China.

His research interest includes the design and optimization of switched reluctance motor.

DA XU received the B.S. and Ph.D. degrees in electrical engineering from Southeast University, Nanjing, China, in 2011 and 2017, respectively.

Since 2017, she has been a member of the faculty in the Nanjing University of Science and Technology (NJUST), where she is currently a Lecturer with the School of Automation. She has authored or coauthored over 30 technical papers and holds three patents in her areas of interest. Her current research interest includes the design and analysis of axial field hybrid excited machine for electric vehicles.

XUEFENG JIANG (S'15–M'17) received the B.S. degree in electrical engineering from Southwest Jiaotong University, Chengdu, China, in 2011, and the Ph.D. degree in electrical engineering from the Nanjing University of Aeronautics and Astronautics (NUAA), Nanjing, China, in 2017.

Since 2017, he has been with the Nanjing University of Science and Technology (NJUST), where he is currently an Assistant Professor with the Department of Electrical Engineering, School of Automation. He has authored or coauthored more than 20 technical papers. He holds more than 20 issued patents. His teaching and research interests include design and control for electric machines, fault diagnosis, and fault-tolerant control for electric drive systems.

WEIWEI GENG received the B.S. degree in electrical engineering from Nanjing Agricultural University (NJAU), Nanjing, China, in 2012, and the M.S. and Ph.D. degrees in electrical engineering from the Nanjing University of Aeronautics and Astronautics (NUAA), Nanjing, China, in 2014 and 2018, respectively.

He is currently with the Department of Electrical Engineering, Nanjing University of Science and Technology (NJUST). He has published more than 15 technical papers in journals and conference proceedings. He has 11 issued/published invention patents. His main research interests include PM machines and control, and electric drive system for electric vehicles and hybrid propulsion.